PNAS RESEARCH ARTICLE | CHEMISTRY
BIOPHYSICS AND COMPUTATIONAL BIOLOGY

In vitro investigation of protein assembly by combined microscopy and infrared spectroscopy at the nanometer scale

Xiao Zhao[a,b,1], Dong Li[c,1], Yi-Hsien Lu[b], Behzad Rad[c], Chunsheng Yan[c], Hans A. Bechtel[d], Paul D. Ashby[c,2], and Miquel B. Salmeron[a,b,2]

Edited by Dennis Discher, University of Pennsylvania, Philadelphia, PA; received January 2, 2022; accepted June 2, 2022 by Editorial Board Member Chad A. Mirkin

The nanoscale structure and dynamics of proteins on surfaces has been extensively studied using various imaging techniques, such as transmission electron microscopy and atomic force microscopy (AFM) in liquid environments. These powerful imaging techniques, however, can potentially damage or perturb delicate biological material and do not provide chemical information, which prevents a fundamental understanding of the dynamic processes underlying their evolution under physiological conditions. Here, we use a platform developed in our laboratory that enables acquisition of infrared (IR) spectroscopy and AFM images of biological material in physiological liquids with nanometer resolution in a cell closed by atomically thin graphene membranes transparent to IR photons. In this work, we studied the self-assembly process of S-layer proteins at the graphene-aqueous solution interface. The graphene acts also as the membrane separating the solution containing the proteins and Ca^{2+} ions from the AFM tip, thus eliminating sample damage and contamination effects. The formation of S-layer protein lattices and their structural evolution was monitored by AFM and by recording the amide I and II IR absorption bands, which reveal the noncovalent interaction between proteins and their response to the environment, including ionic strength and solvation. Our measurement platform opens unique opportunities to study biological material and soft materials in general.

nano-FTIR | operando spectroscopy | S-layer protein | self-assembly | solid-liquid interface

Significance

The growing research in bioengineering calls for in vitro, non-invasive nanoscale characterization of biological macromolecules. However, current imaging tools often use ionizing radiation under high vacuum and/or cold temperature, conditions that are far from the native biological environment. We resolved this challenge by combining nano- Fourier transform infrared spectroscopy (nano-FTIR) with graphene-capped liquid cells that allow us to perform infrared spectroscopy of proteins in their natural liquid environment with nanometer spatial resolution. We monitored the dynamical assembly process and the nanoscale chemical structure of proteins under external stimuli by recording the amide I/II bands in the nano-FTIR absorption spectrum. Our platform opens opportunities for functional studies of soft materials, ranging from biomaterial (enzymes, virus) to polymer material, under in vitro conditions and external stimuli.

The structural and catalytic role of proteins is the foundation of living systems. Most proteins organize into well-defined hierarchical architectures with dynamic interactions (1, 2). Their assembly is governed by protein–protein interactions based on noncovalent hydrogen bonds, hydrophobic, and electrostatic interactions (3). The final form of the protein assembly is sensitive to environmental factors such as pH, ionic strength, and nature of the substrate (4–6).

The self-assembly of proteins has been widely used for biotechnological applications, including sensors, biocatalysts, and in biomaterial synthesis (7, 8). Although substantial effort has been spent to develop spectroscopy and microscopy tools to characterize protein assemblies, including X-ray crystallography, atomic force microscopy (AFM), fluorescence microscopy, and cryo-electron microscopy (9–14), the invasive character of these tools raises concerns about potential alteration of the native structure. Furthermore, these tools primarily offer mostly morphology or structural information, leaving chemical properties and their dynamics largely unexplored. Infrared (IR) spectroscopy, on the other hand, is a nondestructive probe that can reveal their molecular scale structure. In our research we use infrared nanospectroscopy (nano-FTIR), which is based on the plasmonic enhancement of the IR field near the metallic tip of an AFM. This IR near-field decays exponentially away from the tip apex with a characteristic length (in x, y, and z) of the order of the tip radius (around 10–15 nm), thus providing spatial resolution that is ideal to characterize proteins and other biological materials (15, 16). Nano-FTIR has been previously applied by various groups to study biological macromolecules and structures, such as the tobacco mosaic virus (TMV), ferritin, purple membranes (PMs), and phospholipid domains (16–22). However, these studies were performed on dried material in air or with the biomolecules covered with graphene and intercalated water. These nonnative environments can alter the secondary structure of the protein through loss of water or accidental contact by the AFM tip. Bottom illumination method has been used recently, in which the tip is submersed in a liquid cell, but they suffer from strong damping of the tip oscillation due the liquid surrounding the tip and from dragging of the biomolecules, factors that limit its general applicability (20).

We overcame these challenges by developing a liquid cell closed by a graphene membrane that serves as substrate and infrared transparent window. The suspended graphene separates the protein-buffer solution inside the cell from the AFM tip located

The authors declare no competing interest.

This article is a PNAS Direct Submission. D.E.D. is a guest editor invited by the Editorial Board.

[1]X.Z. and D.L. contributed equally to this work.

[2]To whom correspondence may be addressed. Email: pdashby@lbl.gov or mbsalmeron@lbl.gov.

This article contains supporting information online at http://www.pnas.org/lookup/suppl/doi:10.1073/pnas.2200019119/-/DCSupplemental

Published August 1, 2022.

over the membrane in a dry N_2 atmosphere. In this manner, sample damage by tip contact and contamination are eliminated. Photon transparency of single layer graphene ensures minimum attenuation of the tip-enhanced IR near field. The design and fabrication of these cells are described in detail in previous work (23, 24).

The S-layer protein SbpA of the insect bacterium *Lysinibacillus sphaericus* was used as a model system to study biomolecular assembly. SbpA and other S-layer proteins constitute the major external cell component of many bacteria and archaea, serving as exoskeleton and molecular sieve for nutrient uptake (8, 25, 26). The formation is triggered by calcium ions that bind to SbpA forming two-dimensional square lattices of tetrameric unit cells 13 nm in size (12, 27). The assembly process on various substrates, including carbon-based materials such as carbon nanotubes, has been studied in the past using imaging techniques, especially transmission electron microscopy and AFM (10, 12, 28–31).

In this work, we demonstrate that the combination of nano-FTIR spectroscopic imaging with the tip outside the liquid cell and AFM topographic imaging with the tip inside the liquid cell (Fig. 1*A* and *B*) provides structural and chemical information of the proteins with high temporal and spatial resolution. The amide I and amide II bands of the protein were recorded during the assembly process, under different buffer conditions. Their intensities grow nonlinearly vs. time and follow the increase in the area of ordered protein domains obtained from AFM images. The spatial distribution of the amide bands intensities reveals inhomogeneities of the assembly that are not visible in previously reported microscopy results.

Results and Discussion

Fig. 1*A* shows a schematic view of the liquid cell closed by the graphene membrane, where the SbpA proteins adsorb forming two-dimensional lattices, with the AFM tip located outside during acquisition of nano-FTIR spectra. Fig. 1*B* shows a schematic view of the cell for AFM topographic measurements in the same protein-buffer solution, with the tip inside the liquid.

Nano-FTIR spectra of the SbpA protein assembly formed in buffer solutions with different Ca^{2+} concentrations are plotted in Fig. 1*C*. The black trace corresponds to 5 mM Ca^{2+}, the red to 50 mM Ca^{2+}. The blue is an attenuated total reflection FTIR (ATR-FTIR) spectrum of dried assembled SbpA proteins on graphene-coated Au films that serves as reference. Details of data processing of the spectra can be found in the *SI Appendix*. Fig. 1*D* shows AFM topography images of the graphene membrane before (*Left*), and after (*Right*) being covered with SbpA. An expanded image is inserted to show the square structure of the self-assembled protein lattice. The bright features are due to wrinkles in the graphene.

As shown in Fig. 1*C*, the nano-FTIR spectra contain two main peaks, one around 1,660 cm^{-1} and another around 1,550 cm^{-1}.

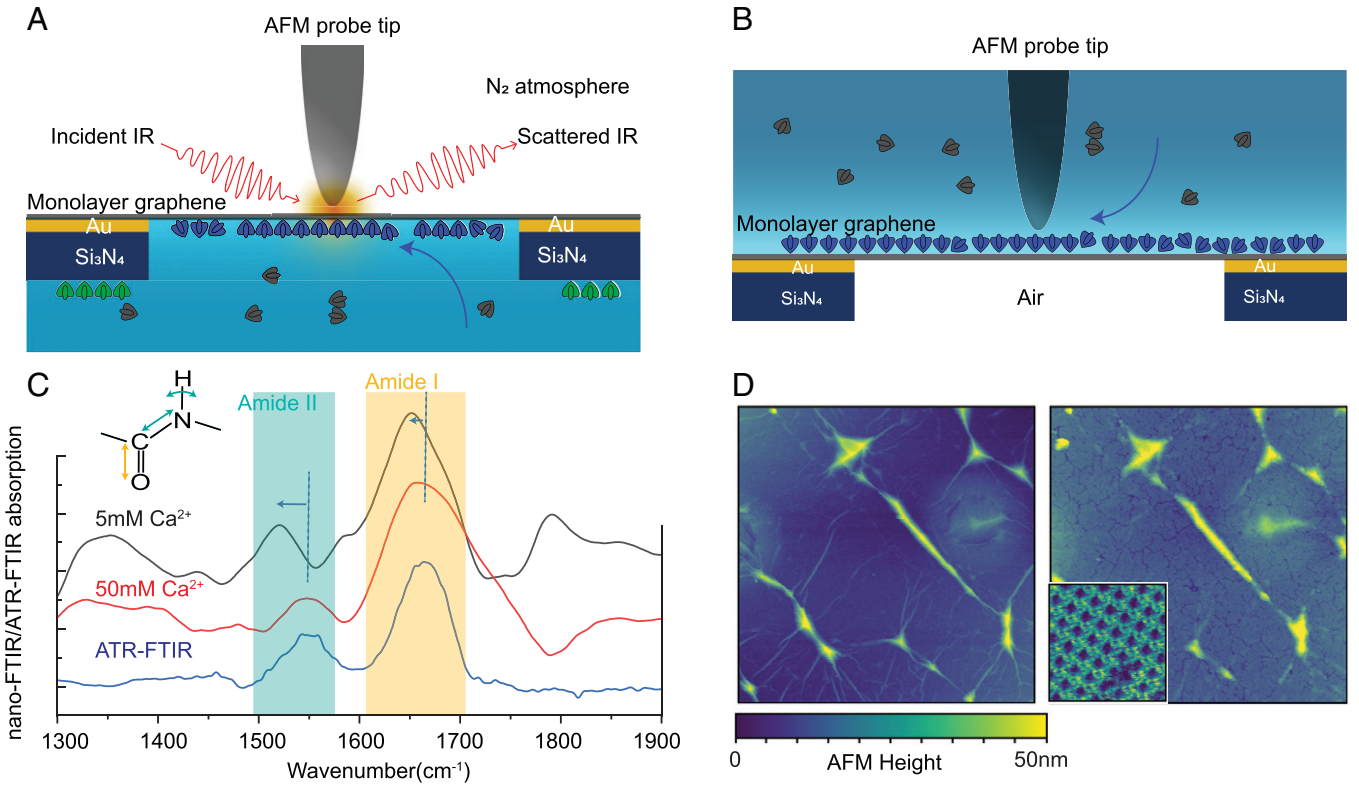

Fig. 1. Schematic drawings of experiment, nano-FTIR spectra, and AFM topographic images of SbpA proteins forming assembly layer. (*A*) Schematic drawing of the nano-FTIR experiment with the AFM tip situated over the monolayer graphene suspended across 1-μm diameter holes of a perforated Si_3N_4 membrane (only one hole is shown). The membrane closes the cell filled with SbpA proteins and Ca^{2+} ions in a buffer solution. The proteins attach to the graphene membrane (colored blue) and Si_3N_4 membrane (colored green) during assembly. Free proteins in the solution are shown in gray. (*B*) Schematic of the high-resolution AFM imaging with the probe immersed in the same protein-buffer solution as in (*A*). (*C*) Nano-FTIR spectra of an assembled film of SbpA proteins in a buffer solution of 5 mM Ca^{2+} (black), and in 50 mM Ca^{2+}(red), acquired 3 h after filling the cell (*Top* two graphs). The *Bottom* graph (blue) is an ATR-FTIR spectrum of dried SbpA proteins assembled from a 50 mM Ca^{2+} solution on a graphene-coated Au film on a Si wafer. The two nano-FTIR spectra are averages of 120–150 spectra collected in different spots of protein-covered regions. (*D*) AFM topographic images of the graphene membrane prior (*Left*) and after SbpA assembly (*Right*) acquired 1 h after filling the cell. The *Inset* is an expanded image showing the square lattice structure of the assembled proteins. The scan size is 3 μm for the large images and 90 nm for the *Inset*. The bright lines are due to wrinkles in the graphene. Protein domains form on both the suspended and supported regions in AFM imaging experiments where the tip scans over the suspended as well as the supported graphene. In the nano-FTIR experiments, only proteins on the suspended graphene can be observed unless damage or detachment of the graphene accidentally occurs.

The first peak has a small contribution from the H_2O bending mode and a larger contribution from the amide I (C = O stretching) mode. The second peak is due to the amide II (N-H bending coupled with C-N stretching) modes. Other peaks are observed below 1,400 cm^{-1} which are attributed to the amide III mode (32), while peaks around 1,800 cm^{-1} (positive for 5 mM and negative for 50 mM) are of unclear origin. These spectra, while overall similar, show several important differences:

First, the center of the amide I and II bands show different red shifts, relative to the ATR reference spectra, as a function of Ca^{2+} concentration. In 5 mM solution, the shifts are 9 cm^{-1} for amide I and 20 cm^{-1} for amide II. In 50 mM buffer solution, the shifts are 5 cm^{-1} for amide I and almost no shift for amide II. This could arise from additional hydrogen bond formation with water molecules (33, 34).

Second, the intensity ratio of the amide I and II band is lower in 50 mM Ca^{2+}. This change can be explained by the polarization of the IR near field, which is roughly oriented along the normal to the surface and thus more sensitive to vibration modes with transition dipole moments perpendicular to the surface (35, 36). The lower intensity of the amide II band might indicate a preferential orientation of the N-H bonds vibration parallel to the surface, which correlates with a stronger ordering of SbpA monomers during self-assembly. Similar results have been reported for the purple membrane (PM) of *Halobacterium salinarum* on silicon substrates and collagen fibril on AuSi substrate by nano-FTIR (16, 18, 37). The change of peak intensity and shifts of the amide bands provide critical information about the protein structural rearrangement during lattice formation (10). We will focus on the amide I and II band intensities and appearance in the following discussion.

Finally, a shoulder peak at higher frequency (near and above 1,700 cm^{-1}), is visible in the 50 mM Ca^{2+} case, which could be due to IR absorption bands of the protein side chains (33). However, since the secondary structure of SbpA includes alpha helices, beta sheets, and beta turns (11, 32), it is difficult at present to assign these IR absorption peaks to different secondary structures.

Assembly Dynamics. The dynamic assembly process of SbpA can be followed from the nano-FTIR spectra on the scale of minutes, the time required to collect one spectrum, while complete assembly of the SbpA takes hours. The top color map in Fig. 2*A* shows the nano-FTIR spectra of SbpA in 5 mM Ca^{2+} buffer solution collected from 0.5 h to 1.5 h after filling the cell with protein solution. The bottom color map shows nano-FTIR spectra acquired in a protein solution without calcium ions. As can be seen, the calcium concentration strongly influences SbpA assembly. In 5 mM Ca^{2+}, after 1.5 h the intensity of the peak around 1,660 cm^{-1} had increased by a factor of 4 compared to its value at 0.5 h and remained nearly constant afterward. The same peak, however, decreased and redshifted in the absence of Ca^{2+}, as shown in the bottom panel. The integrated intensity of the amide I and II bands is plotted in Fig. 2*B* as a function of assembly time (red dots, *Right y* axis). In parallel, AFM images were used to follow the changes in the topography and protein domain size, which is shown in the same Fig. 2*B* (black squares, *Left y* axis). Three AFM images of the protein domains are shown as insets, corresponding to the start, middle, and near the end of the assembly process, respectively.

Several important factors deserve further discussion: first, although both the H_2O bending and amide-I vibration modes contribute to the peak around 1,660 cm^{-1}, the peak intensity increased more than four times during assembly. This increase is due exclusively to the ordering of proteins units, indicating that the bending mode of water contributes less than 25% of the overall peak intensity. The attenuation of the water bending mode will be discussed more thoroughly after the isotopic solvent exchange (H_2O by D_2O) experiments shown below. Second, there are two factors that potentially contribute to the increase of amide I band over time: (i) more protein molecules adsorb on the graphene substrate, and (ii) gradual ordering of the adsorbed protein forming the crystalline phase, which orients its dynamic dipole more perpendicular to the surface. Since the adsorption (not the crystallization) took several minutes to complete, well before the nano-FTIR measurements, it is unlikely that increased adsorption is the major contribution (10, 12). Third, the area of assembled protein, obtained from the AFM topography images, shows a larger percentage of ordered domains at later times, indicating a good agreement between these two measurements.

Spatially Resolved Chemical Mapping During Protein Assembly. Calcium ions are essential for driving and stabilizing the crystallization of the S-layer protein monomeric units (5, 11, 27). The evolution of the SbpA protein self-assembly process therefore

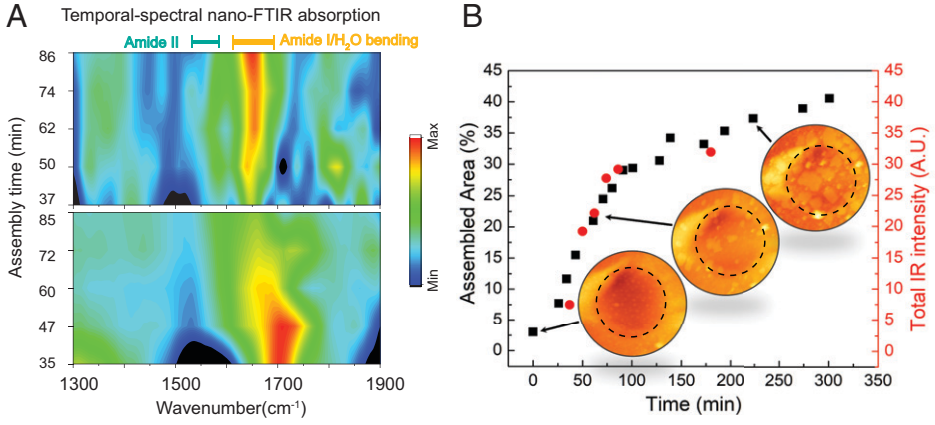

Fig. 2. Temporally resolved assembly process of SbpA protein. (*A*) Color map representation of the time evolution of the nano-FTIR spectra during SbpA protein assembly on the graphene membrane in a buffer solution of 5 mM Ca^{2+} (*Top*), and without Ca^{2+} (*Bottom*). The tip location was fixed during the measurement. (*B*) Percentage of area covered by assembled protein from AFM images in 5 mM Ca^{2+} buffer solution (black squares, *Left y* axis). Integrated intensity of Amide I and Amide II bands (red dots, *Right y* axis) from the spectra shown in the top panel of (*A*). The three circular insets are AFM images showing SbpA domain growth on the graphene membrane as a function of time. Time 0 corresponds to the introduction of the protein/buffer solution into the cell. The suspended graphene boundary is marked by black dashed circles.

depends on the Ca^{2+} concentration, as shown in Fig. 3. Fig. 3*A* and *C* show images of the total near-field IR amplitude scattered by the tip as it scans over the graphene-covered holes and surrounding regions. The intensity increases when the probe is outside the suspended graphene window because of the strong scattering of all wavelengths by the underlaying gold. Nano-FTIR spectra acquired along the lines marked by the red arrows in (*A*) and (*C*) are presented as color maps in Fig. 3*B* and *D*. In both cases, the spectra were collected 3 h after start of the assembly process, when the assembly process is nearly complete and the amount of SbpA monomers in the solution has been depleted. In both 5 mM Ca^{2+} and 50 mM Ca^{2+} solutions, the intensity of the amide I/II bands vary as the tip scans over domains formed at the graphene-solution interface. At least three different domains are visible in the 5 mM case and two in the 50 mM case, (marked by red segments). The size of these domains is a few 100 nm, close to the domain size measured in AFM topography images (Fig. 2*B*). The differences in spectra between different domains, especially in the amide II band, suggest structural variation between domains. For example, the weakening of amide II band in domain II in 50 mM (Fig. 3*D*) is in line with the reorientation of protein lattice units discussed above.

Effect of Solvent Replacement. Hydrogen-deuterium exchange experiments have been used widely in biological research to probe the folding pathways and conformational changes of proteins and their interactions (38–40). We therefore studied the effect of deuterium substitution on the protein assembly by replacing the 5 mM Ca^{2+} H_2O buffer solution in the liquid cell with 5 mM Ca^{2+} D_2O buffer solution 3 h after completion of the assembly process. Fig. 4*A* is an AFM topographic image of a region showing a graphene-covered hole, after replacing the H_2O solution with a D_2O solution using a gentle slow flow of the solution to avoid turbulence or high shear flow. Fig. 4*C* corresponds to another experiment using an energetic rinse with a 5 mM $Ca^{2+}D_2O$ solution. The corresponding nano-FTIR spectra along the red line arrows are shown as color maps in Fig. 4*B* and *D*.

After the gentle solution replacement, most of the self-assembled protein remained at the graphene-solution interface, although with a substantial change in the amide II band in the nano-FTIR spectrum. The amide II band is sensitive to H/D exchange because of the conversion of NH bonds to ND bonds, which have a lower frequency (33, 41, 42). As a result, the decoupled amide-II band shifted to 1,450 cm^{-1}, which is mostly due to the CN stretching mode, as seen in Fig. 4*B*. The bending mode of D_2O (around 1,220 cm^{-1}, visible in Fig. 4*D*), however, is very weak or not observed in the nano-FTIR spectrum. This is because the nano-FTIR technique only probes vibrations within the decay length of the IR near field, which is usually 10–15 nm (i.e., roughly the tip radius of curvature or our tip) (16). Thus, the penetration of the IR near field through the protein assembly layer plus graphene, approximately 10 nm, is very small, shading the underlying D_2O, which did not intercalate between self-assembled protein domains and graphene.

However, the turbulent D_2O rinse altered the structure of the graphene window, first by detaching it from the surrounding gold support which allowed intercalation of water between the two (Fig. 4*C*). It also removed a large amount of protein, as shown in

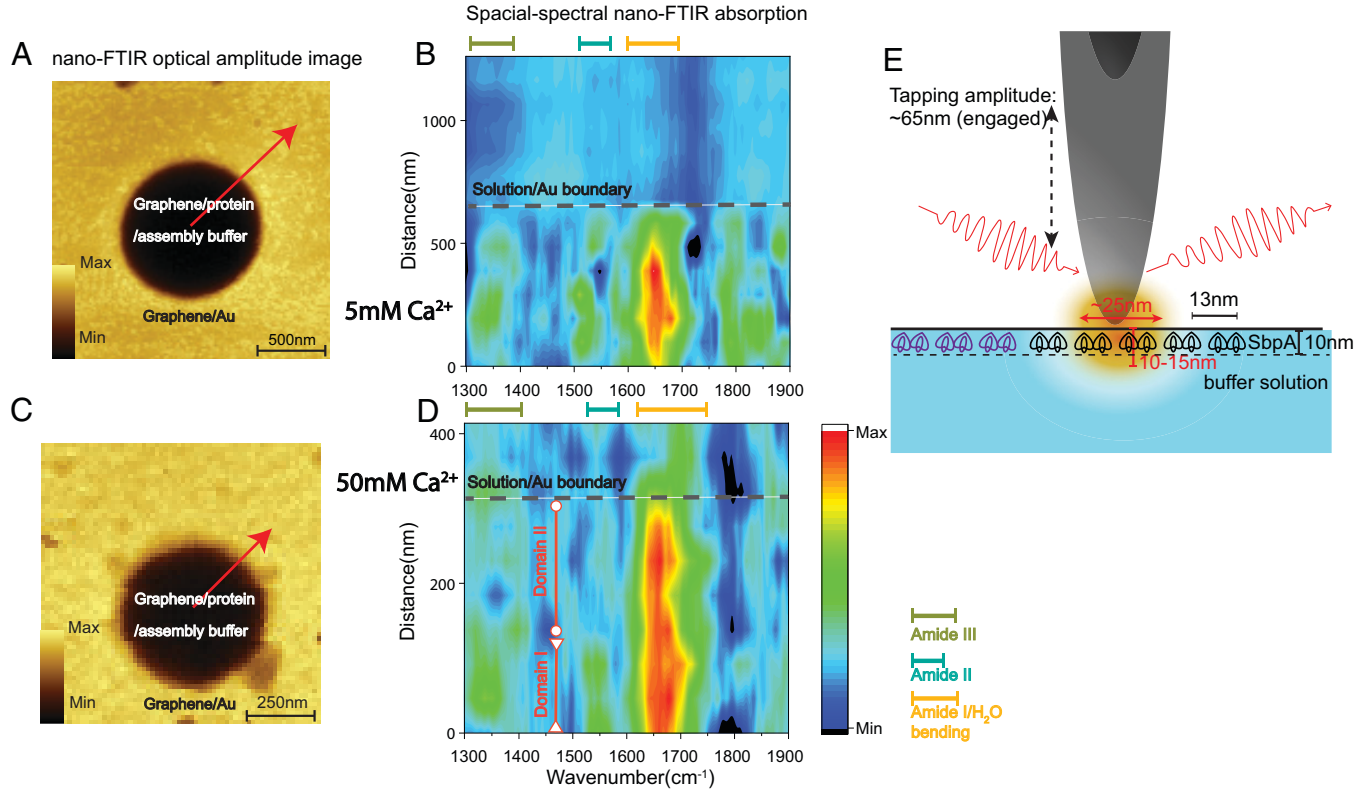

Fig. 3. Spatially resolved chemical mapping of SbpA protein assemblies. (*A* and *B*) Images of the total scattered optical amplitude of suspended graphene and surrounding area in the cell filled with SbpA proteins, in 5 mM Ca^{2+} buffer solution in (*A*) and 50 mM Ca^{2+} solution in (*C*). Total optical amplitude increases substantially when the probe is over the gold substrate. (*B* and *D*) Corresponding color map representations of the nano-FTIR spectral intensities (arbitrary units in the color scale) of the amide I and II mode regions of the SbpA proteins. The nano-FTIR profiles were acquired at positions along the red arrows in (*A*) and (*C*). The amide I and II modes are only visible when the tip is located over the suspended graphene region in contact with the solution. The hole boundary is marked by the horizontal dashed lines. The position of two self-assembled domains in (*D*) is marked by the vertical red segments. (*E*) Schematic drawing of the tip-sample junction showing exponential the decay of the IR near field away from the tip apex. A SbpA lattice is drawn for comparison.

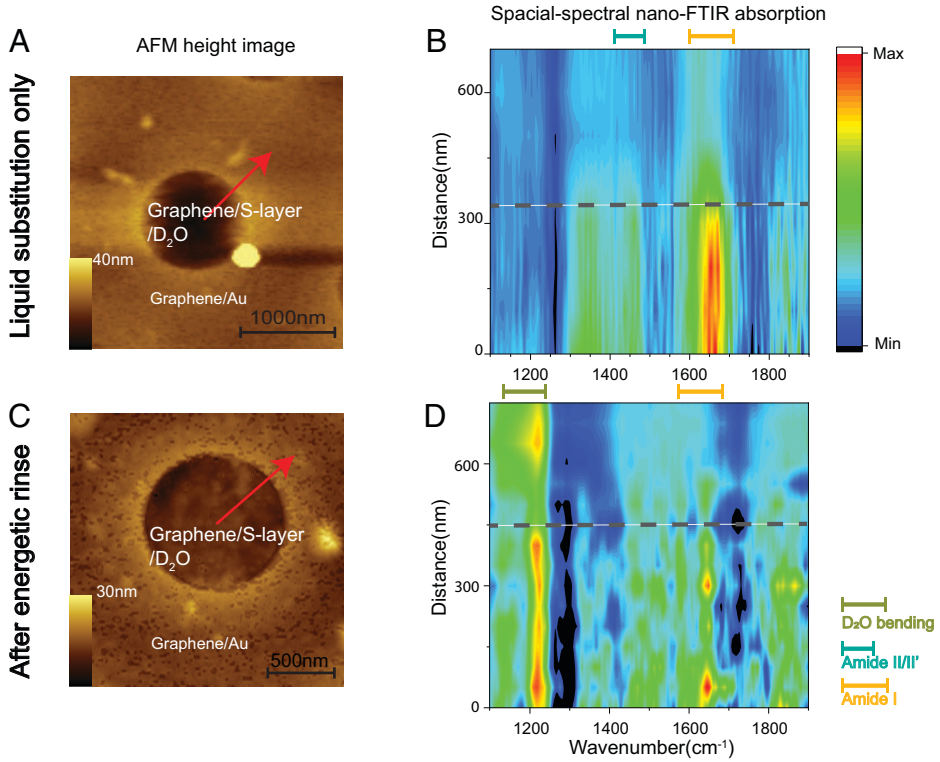

Fig. 4. Effect of solvent replacement on SbpA proteins. (*A*) AFM topographic image of an area containing a graphene covered hole in the cell filled with SbpA proteins after gently substituting 5 mM Ca^{2+} H_2O solution for 5 mM Ca^{2+} D_2O solution. (*B*) Color map representation of the nano-FTIR spectra along the line marked by the red arrow in (*A*). The D_2O bending mode at 1,220 cm^{-1} is very weak indicating that D_2O did not intercalate between the protein domain and graphene. (*C*) AFM topographic image after a turbulent rinsing with D_2O that perturbed both the protein layers and the graphene membrane. (*D*) Color map representation along the direction of red arrow in (*C*). The appearance of an intense D_2O bending mode at 1,220 cm^{-1}, along with the weaker amide peaks in the graphene-covered hole region after the energetic rinsing, indicates that D_2O replaced H_2O and largely removed the initial protein layer covering the graphene. In addition, the D_2O peak is also visible even outside the suspended region due to intercalation between graphene and the surrounding Au film. The negative band around 1,270 cm^{-1} (dark blue) in both cases is due to contamination of the AFM cantilever and tip with PDMS, which has a characteristic peak in that region.

the nano-FTIR line profile (Fig. 4*D*), leaving only small protein domains on the surface, as evidenced by the intensity profile of the amide-I band. These line scans further demonstrate the promising application of our platform to resolve biological nanostructures and their chemical changes down to tens of nanometers.

Conclusion and Summary

It is clear then that our graphene-based platform combined with AFM and nano-FTIR makes possible in vitro studies of the structural and chemical evolution of biological material, exemplified here by the study of the self-assembly of SbpA proteins on graphene. The growth of amide I and II band intensities of SbpA protein follows a nonlinear behavior vs. time, in good agreement with the dynamical information obtained from AFM topographic images. After assembly, the amide band line profile unambiguously reveals the structural response of protein to environmental factors, including ionic strength and solvent, which is hard to access by AFM. We have shown that the dynamical evolution of the protein substructure depends on the environment. We have also shown the interaction existing between proteins and matrix. Finally we have shown that the protein-substrate and protein-water interactions can be studied using our approach. The nm spatial resolution, chemical sensitivity, negligible radiation damage, and environmental capabilities of our platform open many opportunities to study other complex soft materials and nanostructures.

With the advance of fabrication technology, the spatial resolution, which is correlated to the tip apex radius, can be further increased, and we anticipate that dynamic IR spectroscopic study of a single protein or DNA molecule during the execution of its biological function will be possible in the future.

Materials and Methods

Wild-Type SbpA Expression and Purification. Detailed expression and purification procedure of wild-type SbpA can be found in previously published work (27, 43). In general, *Lysinibacillus sphaericus CCM2177* cells (ATCC No.4525) were inoculated from glycerol stock and grown in a 20 mL SVIII culture medium at 32 °C overnight. Then the overnight culture was expanded to 500 mL SVIII medium at 32 °C for 6–7 h (OD_{600} = 0.7–1.0, OD refers to optical density). After reaching the desired OD, the cells were harvested by spinning down in JLA 8.1 centrifuge rotor at 15,000 × *g* for 20 min at 4 °C. The cell pellets were resuspended in cold 50 mM Tris HCl buffer at pH 7.2. An EmulsiFlex-C3 homogenizer (Avestin) was used to lyse the suspended cells at 20,000 psi. A JA-20 rotor was used to pellet cell walls at 28,000 × *g* for 15 min, and the upper, lighter pellet (the cell walls) was collected by a plastic spatula. The lower, darker pellet (unbroken cells) was again suspended in Tris buffer, ultrasonically treated, and spun down. This procedure was repeated four times. The crude cell-wall preparations (collected pellets) were extracted with 250 mL of 0.75% Triton X-100 to remove contaminating plasma membrane fragments and stirred for 10 min at room temperature (22 ± 2 °C). Subsequently, the cell-wall fragments were sedimented at 40,000 × *g* for 10 min. The extraction step was repeated three times. The purified cell wall fractions were denatured using a solution of 50 mM Tris HCl pH 7.2, and 5 M guanidine hydrochloride for 30 min. SbpA was dialyzed extensively into Milli-Q water (EMDMillipore, Billerica). Aggregated protein was removed by a final centrifugation at 100,000 × *g* at 4 °C in an Optima L-100XP ultracentrifuge (Beckman Coulter) using the SW41 Ti rotor. Protein concentrations were determined through Beer's law using the calculated molar extinction coefficient at 280 nm of 78,940 $M^{-1}cm^{-1}$ or the weight extinction coefficient of 0.6 $(mg/mL)^{-1}$ cm^{-1}. Purified SbpA was present as a monomer with a

hydrodynamic diameter of 11.7 ± 0.5 nm, and upon addition of Ca^{2+}, the protein crystallized into a porous, square lattice with a cell spacing of 13.2 ± 0.2 nm.

Graphene Membrane. The details of graphene membrane fabrication can be found in previous work (23, 24). In brief, commercial single-layer graphene grown on Cu foil (Graphene Factory) by chemical vapor deposition was used as base material. Residual graphene on the other side of the foil was removed by O_2 plasma. An adhesive Al foil frame window was stuck to the untreated side and then floated on a Cu etchant solution (~90 mL 0.2 M sodium persulfate). After etching out the Cu, the graphene with Al window frame was transferred to a deionized water reservoir (~500 mL) to remove salt residues. The transfer process to the water reservoir was repeated twice to ensure complete salt removal. A Cr (2.5 nm)/Au (25 nm)-coated SiN membrane (100 nm thickness) perforated with an array of 1,000 nm or 500 nm circular holes (Norcada) was placed in the reservoir underneath the graphene and carefully lifted up from the air/water interface to complete the graphene transfer. After this the membranes were annealed in vacuum (lower than 10^{-6} torr) up to 573 K to increase the adhesion between graphene and Au.

ATR-FTIR. The S-layer protein was assembled in buffer solution with 50 mM Ca^{2+} on graphene coated 70 nm Au/Si (using the same graphene transfer method described above) and dried under nitrogen flow. The ATR-FTIR measurements were conducted by a Thermo Nicolet iS50 FTIR spectrometer with a diamond crystal ATR module. The spectra were collected with 4 cm^{-1} resolution in the spectral range from 4,000 cm^{-1} to 400 cm^{-1} averaging over 64 scans and normalized to the light intensity.

AFM in Liquid. In situ atomic force microscopy was performed on an Asylum Cypher AFM equipped with a fluid cell using soft tapping mode in liquid. The AFM probe consisted of a sharp silicon tip on a silicon nitride cantilever (BioLever mini, BL-AC40TS) with a spring constant of 0.09 N/m. In a typical SbpA assembly experiment, WT SbpA stock solution (4 mg/mL) in pure water and assembly buffer solution (100 mM NaCl, 10 mM Tris, 5 mM $CaCl_2$, pH 7.2) were mixed (1:20 ratio), and the mixed solution was delivered into the AFM liquid cell using a syringe pump. The assembly reaction was monitored at room temperature for 4 h. AFM images were collected at line frequencies of 0.5–1 Hz.

Seal and Rinse. The protein solution and assembly buffer solution (1:20 ratio) were mixed and sealed in the graphene liquid cell just before experiment started (time 0). For solvent change experiment without turbulence rinse, the liquid cell was disassembled and the liquid inside the cell was replaced by 5 mM Ca^{2+} in D_2O solution. The membrane was kept wet during the solvent exchange. For solvent change experiment with turbulence rinse, the membrane was washed by 5 mM Ca^{2+} in D_2O solution several times before sealing. The cell was then sealed again for experiment.

Nano-FTIR. Nano-FTIR measurements were performed at beamline 2.4 and 5.4 of the Advanced Light Source, at the Lawrence Berkeley National Laboratory. The infrared light was focused onto the Pt-coated AFM tip in a neaSNOM (Neaspec) system. Tapping-mode operation was performed at the fundamental resonance frequency of the cantilever (250–350 kHz) with a free oscillation amplitude ranging from 70 to 90 nm and an amplitude setpoint of ~80%. The scattered near-field signal is retrieved by a lock-in amplifier tuned to the second and higher harmonics of the cantilever oscillation to eliminate the far field nonlocal scattered background. The complex-valued near-field spectrum is derived from a Fourier transform of the interferogram. The Fourier components are presented as real spectral amplitude "A" and phase "∅", normalized to reference spectra obtained with the tip outside the hole: $A_i(v) = A_i^{\text{sample}}(v)/A_i^{\text{reference}}(v)$ and $\emptyset_i(v) = \emptyset_i^{\text{sample}}(v) - \emptyset_i^{\text{reference}}(v)$ where v is the wavenumber. Reference spectra were taken on samples with flat spectral responses, either Au-coated Si or graphene on the Au-coated SiN membrane. The spectra displayed throughout the paper is the phase φ_2 of the scattered signal at the second harmonic of the cantilever oscillation frequency, which has been shown to be in good agreement with traditional FTIR absorption measurements. A third order polynomial background has been subtracted from each nano-FTIR absorption spectrum. The negative band around 1,270 cm^{-1} (such as that in Fig. 4) in both cases is due to contamination of the AFM cantilever and tip with polydimethylsiloxane (PDMS), which has a characteristic peak in that region.

Data Availability. All study data are included in the article and *SI Appendix*.

ACKNOWLEDGMENTS. This work was funded by the US Department of Energy, Office of Science, Office of Basic Energy Sciences, Materials Sciences and Engineering Division (DE-AC02-05-CH11231) program Unlocking Chemical Circularity in Recycling by Controlling Polymer Reactivity Across Scales CUP-LBL-Helms. This research used resources of the Advanced Light Source, a Department of Energy (DOE) Office of Science User Facility (DE-AC02-05-CH11231). Nano-FTIR was performed at beamline 2.4 and 5.4 in ALS, and AFM and protein preparation were performed at the Molecular Foundry, supported by the DOE Office of Basic Energy Sciences under the same contract number. X.Z. was supported by a National Science Foundation-Binational Science Foundation (1906014).

Author affiliations: [a]Department of Materials Science and Engineering, University of California at Berkeley, Berkeley, CA 94720; [b]Materials Sciences Division, Lawrence Berkeley National Laboratory, Berkeley, CA 94720; [c]Molecular Foundry, Lawrence Berkeley National Laboratory, Berkeley, CA 94720; and [d]Advanced Light Source, Lawrence Berkeley National Laboratory, Berkeley, CA 94720

Author contributions: X.Z., D.L., Y.-H.L., B.R., P.D.A., and M.B.S. designed research; X.Z., D.L., Y.-H.L., and C.Y. performed research; X.Z. and H.A.B. contributed new reagents/analytic tools; X.Z., D.L., H.A.B., P.D.A., and M.B.S. analyzed data; and X.Z., D.L., H.A.B., P.D.A., and M.B.S. wrote the paper.

1. Q. Luo, C. Hou, Y. Bai, R. Wang, J. Liu, Protein assembly: versatile approaches to construct highly ordered nanostructures. *Chem. Rev.* **116**, 13571–13632 (2016).
2. Y. Bai, Q. Luo, J. Liu, Protein self-assembly via supramolecular strategies. *Chem. Soc. Rev.* **45**, 2756–2767 (2016).
3. J. J. McManus, P. Charbonneau, E. Zaccarelli, N. Asherie, The physics of protein self-assembly. *Curr. Opin. Colloid Interface Sci.* **22**, 73–79 (2016).
4. X. Y. Wang *et al.*, A S-layer protein of *Bacillus anthracis* as a building block for functional protein arrays by in vitro self-assembly. *Small* **11**, 5826–5832 (2015).
5. U. B. Sleytr, B. Schuster, E.-M. Egelseer, D. Pum, S-layers: principles and applications. *FEMS Microbiol. Rev.* **38**, 823–864 (2014).
6. B. Schuster, U. B. Sleytr, Biomimetic interfaces based on S-layer proteins, lipid membranes and functional biomolecules. *J. R. Soc. Interface* **11**, 20140232 (2014).
7. R. P. Fagan, N. F. Fairweather, Biogenesis and functions of bacterial S-layers. *Nat. Rev. Microbiol.* **12**, 211–222 (2014).
8. U. B. Sleytr, P. Messner, D. Pum, M. Sara, *Crystalline Bacterial Cell Surface Proteins* (Elsevier, 1996).
9. J. Herrmann *et al.*, A bacterial surface layer protein exploits multistep crystallization for rapid self-assembly. *Proc. Natl. Acad. Sci. U.S.A.* **117**, 388–394 (2020).
10. S.-H. Shin *et al.*, Direct observation of kinetic traps associated with structural transformations leading to multiple pathways of S-layer assembly. *Proc. Natl. Acad. Sci. U.S.A.* **109**, 12968–12973 (2012).
11. E. Baranova *et al.*, SbsB structure and lattice reconstruction unveil Ca2+ triggered S-layer assembly. *Nature* **487**, 119–122 (2012).
12. S. Chung, S.-H. Shin, C. R. Bertozzi, J. J. De Yoreo, Self-catalyzed growth of S layers via an amorphous-to-crystalline transition limited by folding kinetics. *Proc. Natl. Acad. Sci. U.S.A.* **107**, 16536–16541 (2010).
13. A. M. Vrabioiu, T. J. Mitchison, Structural insights into yeast septin organization from polarized fluorescence microscopy. *Nature* **443**, 466–469 (2006).
14. G. Obal *et al.*, STRUCTURAL VIROLOGY. Conformational plasticity of a native retroviral capsid revealed by x-ray crystallography. *Science* **349**, 95–98 (2015).
15. H. A. Bechtel, S. C. Johnson, O. Khatib, E. A. Muller, M. B. Raschke, Synchrotron infrared nano-spectroscopy and-imaging. *Surf. Sci. Rep.* **75**, 100493 (2020).
16. H. A. Bechtel, E. A. Muller, R. L. Olmon, M. C. Martin, M. B. Raschke, Ultrabroadband infrared nanospectroscopic imaging. *Proc. Natl. Acad. Sci. U.S.A.* **111**, 7191–7196 (2014).
17. O. Khatib *et al.*, Graphene-based platform for infrared near-field nanospectroscopy of water and biological materials in an aqueous environment. *ACS Nano* **9**, 7968–7975 (2015).
18. I. Amenabar *et al.*, Structural analysis and mapping of individual protein complexes by infrared nanospectroscopy. *Nat. Commun.* **4**, 2890 (2013).
19. V. J. Rao *et al.*, AFM-IR and IR-SNOM for the characterization of small molecule organic semiconductors. *J. Phys. Chem. C* **124**, 5331–5344 (2020).
20. E. Pfitzner, J. Heberle, Infrared scattering-type scanning near-field optical microscopy of biomembranes in water. *J. Phys. Chem. Lett.* **11**, 8183–8188 (2020).
21. K. J. Kaltenecker, T. Gölz, E. Bau, F. Keilmann, Infrared-spectroscopic, dynamic near-field microscopy of living cells and nanoparticles in water. *Sci. Rep.* **11**, 21860 (2021).
22. L. M. Meireles *et al.*, Synchrotron infrared nanospectroscopy on a graphene chip. *Lab Chip* **19**, 3678–3684 (2019).
23. Y.-H. Lu *et al.*, Ultra-thin free-standing oxide membranes for electron and photon spectroscopy studies of solid-gas and solid-liquid Interfaces. *Nano Lett.* (2020).
24. Y.-H. Lu *et al.*, Infrared nanospectroscopy at the graphene-electrolyte interface. *Nano Lett.* **19**, 5388–5393 (2019).
25. N. Ilk, E. M. Egelseer, U. B. Sleytr, S-layer fusion proteins–Construction principles and applications. *Curr. Opin. Biotechnol.* **22**, 824–831 (2011).
26. M. Sára, U. B. Sleytr, S-layer proteins. *J. Bacteriol.* **182**, 859–868 (2000).
27. B. Rad *et al.*, Ion-specific control of the self-assembly dynamics of a nanostructured protein lattice. *ACS Nano* **9**, 180–190 (2015).
28. A. Breitwieser, P. Siedlaczek, H. Lichtenegger, U. B. Sleytr, D. Pum, S-layer protein coated carbon nanotubes. *Coatings* **9**, 492 (2019).

29. M. Charrier *et al.*, Engineering the S-layer of *Caulobacter crescentus* as a foundation for stable, high-density, 2D living materials. *ACS Synth. Biol.* **8**, 181–190 (2019).
30. B. Stel, F. Cometto, B. Rad, J. J. De Yoreo, M. Lingenfelder, Dynamically resolved self-assembly of S-layer proteins on solid surfaces. *Chem. Commun. (Camb.)* **54**, 10264–10267 (2018).
31. B. Stel *et al.*, Contrasting chemistry of block copolymer films controls the dynamics of protein self-assembly at the nanoscale. *ACS Nano* **13**, 4018–4027 (2019).
32. P. Mobili *et al.*, Characterization of S-layer proteins of *Lactobacillus* by FTIR spectroscopy and differential scanning calorimetry. *Vib. Spectrosc.* **50**, 68–77 (2009).
33. A. Barth, Infrared spectroscopy of proteins. Biochim. Biophys. Acta (BBA). *Bioenerget.* **1767**, 1073–1101 (2007).
34. D. Paschek *et al.*, The solvent-dependent shift of the amide I band of a fully solvated peptide as a local probe for the solvent composition in the peptide/solvent interface. *ChemPhysChem* **9**, 2742–2750 (2008).
35. E. A. Muller, B. Pollard, H. A. Bechtel, P. van Blerkom, M. B. Raschke, Infrared vibrational nanocrystallography and nanoimaging. *Sci. Adv.* **2**, e1601006 (2016).
36. A. V. Zayats, D. Richards, *Nano-Optics and Near-Field Optical Microscopy* (Artech House, 2009).
37. G. Bakir *et al.*, Orientation matters: Polarization dependent IR spectroscopy of collagen from intact tendon down to the single fibril level. *Molecules* **25**, 4295 (2020).
38. S. W. Englander, L. Mayne, Z.-Y. Kan, W. Hu, Protein folding–How and why: By hydrogen exchange, fragment separation, and mass spectrometry. *Annu. Rev. Biophys.* **45**, 135–152 (2016).
39. M. Guttman *et al.*, Antibody potency relates to the ability to recognize the closed, pre-fusion form of HIV Env. *Nat. Commun.* **6**, 6144 (2015).
40. J. G. Mandell, A. Baerga-Ortiz, A. M. Falick, E. A. Komives, *Protein-Ligand Interactions* (Springer, 2005), pp. 65–79.
41. S. Krimm, J. Bandekar, Vibrational spectroscopy and conformation of peptides, polypeptides, and proteins. *Adv. Protein Chem.* **38**, 181–364 (1986).
42. K. A. Oberg, J. M. Ruysschaert, E. Goormaghtigh, The optimization of protein secondary structure determination with infrared and circular dichroism spectra. *Eur. J. Biochem.* **271**, 2937–2948 (2004).
43. B. Schuster, E. Györvary, D. Pum, U. B. Sleytr, Nanotechnology with S-layer proteins. *Protein Nanotechnol.* 101–123 (2005).